Scandium $K\alpha$ and $K\beta$ x-ray spectra with *ab initio* satellite intensities and energy eigenvalues

J. W. Dean ⊙,[*] H. A. Melia ⊙,[†] T. V. B. Nguyen ⊙,[‡] and C. T. Chantler ⊙[§]

The University of Melbourne, Parkville, Victoria 3010, Australia

Characteristic x-ray spectra offer insight into the structure and composition of atoms and molecules at a fundamental level where discrepancies in asymmetry, peak energy, and shape between theory and experiment motivate investigations. This work calculates highly convergent electron wavefunctions using the multiconfiguration Dirac-Hartree-Fock method and reveals the capability of recreating x-ray spectra from first principles, with eigenvalue convergence of order 0.1 eV and amplitude convergence of order 1–4%. The canonical $K\alpha$ and $K\beta$ transitions, $[1s] \rightarrow [2p]$ and $[1s] \rightarrow [2p]$, respectively, where square brackets denote hole states, are not sufficient to recreate major features present in the data. Shake-off satellites, where the transitions take place in the presence of a secondary nl hole, are necessary to account for observed asymmetries. The probabilities for these shake-off events are determined and used to obtain *ab initio* satellite intensities. The Auger effect is considered for these satellite intensities through an Auger suppression factor. This work presents the full energy eigenvalue spectrum for several scandium transitions: $[1s^2]$ hypersatellites ($K\alpha^h$ and $K\beta^h$), the $n = 2$ $K\alpha_{3,4}$ and $K\beta$ equivalent satellites, and double shake-off satellites. Calculations are compared with deconvolved experimental data using several fitting models which yield compelling goodness of fit $\chi_r^2 = 1.14$ for $K\alpha$ and $\chi_r^2 = 1.72$ for $K\beta$. The selected best model is chosen through the statistical F-test and this model is fitted with raw (not deconvolved) experimental data with $\chi_r^2 = 0.92$ ($K\alpha$) and $\chi_r^2 = 1.31$ ($K\beta$).

I. INTRODUCTION

Investigations of characteristic atomic spectra have been central to the modern physics of each generation from Bohr's model to relativistic effects found in spin splitting fine structures and investigations of the proton radius [1]. Performing theoretical calculations from first principles for characteristic x-ray spectra of atoms is an essential part of quantum mechanics, atomic physics, and quantum electrodynamics (QED). Further to studies into fundamental physics, the ability to reconstruct x-ray spectra has industrial applications wherever x-ray fluorescence (XRF) is important, such as biology [2], food science [3], nanomaterials [4], geochemistry [5], archaeology [6], and environmental science [7].

Satellites in x-ray spectra are observed as a profile with a degenerate energy centroid to the main, or diagram, profile. Often satellite lines are inferred due to the presence of asymmetries within a single profile which implies the existence of several non-well-resolved spectra. A satellite line was first observed by Siegbahn and Stenstrom [8–12]. Wentzel proposed the shake-off hypothesis to explain satellites, where a secondary electron is emitted into the continuum during the initial ionization altering the potential the $K\alpha$ transitions ($2p \rightarrow 1s$) take place in. Bloch [13] applied the sudden, or adiabatic, approximation to calculations of shake events, which was expanded on by Åberg [14].

To calculate the probability of a shake-off event the sudden or adiabatic approximation is used. This states that the cross section for an initial and final atomic wavefunction is independent of the kinetic energy of the initial perturbation, or the transition takes place with no intermediate wavefunction. During the initial perturbation of the core electron, $1s$ for a K transition, another electron from some nl shell is ejected into the continuum. This alters the canonical $K\alpha$ transitions from hole states $[1s] \rightarrow [2p]$ to an nl shake-off satellite transition of $[1snl] \rightarrow [2pnl]$, and similarly for $K\beta$ and all other characteristic spectra, where square brackets denote hole states.

Calculations performed *a priori* for shake-off spectra are scarce and, when performed, rely on significant simplifications. This is due to the presence of complex spin-coupling states from extra electron holes in an open-shell core hole quantum state. When shake-off spectra are modeled, they typically have free relative intensities, limiting the strength with which one can claim that shake events definitively create satellite lines and asymmetries [15].

Over the last three decades, investigations for copper $K\alpha$ have been fruitful, especially because Cu $K\alpha$ is the most well measured of all x-ray spectra, providing an ideal forum for theoretical inquiry [16–28]. Unlike copper, scandium studies are rare. It is not a dominant laboratory x-ray fluorescence source and its low-energy x rays make crystal diffraction difficult, yet it is important for mining and chemical applications [29,30]. There are few works measuring scandium characteristic x-ray spectra [31–37]. Only three studies perform theoretical investigations of scandium x-ray spectra [15,33,38]. In the most recent of these, Dean *et al.* [15] computed eigenvalues for scandium $K\alpha$ and $K\beta$— including the diagram lines, the $n = 3$ satellite lines, and

[*]jonathan.dean@unimelb.edu.au

[†]h.melia@student.unimelb.edu.au

[‡]nguyentvb@gmail.com

[§]chantler@unimelb.edu.au

the 4s satellite line. However, they did not obtain *ab initio* shake-off probabilities, nor high-energy satellites, nor double shake-off satellites. Scandium offers unique insight into theoretical studies of computational atomic physics due to its lone $3d$ electron which can exist in many quantum states, $m_\ell \in \{-2, -1, 0, 1, 2\}$. This provides many possible spin-coupling states, which add complexity to the computations and therefore a strong test of the capabilities of state-of-the-art atomic physics.

This work is directly relevant for the wider x-ray physics community [39], Auger electron spectra [40], shake-up satellites in photoelectron spectra [41], synchrotron science studies [42], and x-ray free electron laser studies [43]. It demonstrates the potential for accurate characterization and diagnosis of rare earth elements [44], cognate with scandium. Furthermore, the methods outlined in this work and the advances in the multiconfiguration Dirac-Hartree-Fock method are of interest in fields including atomic clocks [45,46], QED-sensitive transitions [47], and hyperfine transitions [48].

II. THEORY

We use the multiconfiguration Dirac-Hartree-Fock (MCDHF) framework to calculate the transition eigenenergies and relative probabilities of the diagram and shake-off satellite lines [49,50]. This method is well tested in many fields including highly charged ions [51], photoionization studies [52], high-Z elements [53], physical chemistry [54], and atomic physics [55,56]. MCDHF calculations are performed iteratively to achieve self-consistent wavefunctions minimizing the Dirac Hamiltonian:

$$H_D = c\boldsymbol{\alpha} \cdot \boldsymbol{p} + \beta mc^2 + V(r) \tag{1}$$

for the Hermitian 4×4 matrices $\alpha_1, \alpha_2, \alpha_3$, and β, the particle momentum $\boldsymbol{p}$, and some potential $V(r)$.

This work uses the GRASP software package [57], which is well documented [57–59] and has proven successful in providing good understanding of experimental atomic spectra [60] and other studies [61,62]. The finite size of the nucleus is accounted for [49,63]. Our implementation of the GRASP software includes an Lowe-Chantler-Grant-Welton self-energy [64] and self-energy screening approximations [65].

The Hartree-Fock, or self-consistent field, method is a process for approximating the wavefunction for a many-body system. It has widespread use in computational physics and chemistry for obtaining wavefunctions for complex molecules [66] and nuclear physics with the Hartree-Fock-Bogoliubov method [67]. It can use different forms of the initial wavefunction, such as Gaussian orbitals [68], and can solve for wavefunctions in the presence of strong electric fields [69].

In spherical polar coordinates, (r, θ, φ), eigenstates of the Dirac Hamiltonian from Eq. (1) have the 4-spinor form

$$\phi(r, \theta, \varphi) = \frac{1}{r}\begin{pmatrix} P(r)\chi_{\kappa m}(\theta, \varphi) \\ iQ(r)\chi_{-\kappa m}(\theta, \varphi) \end{pmatrix}, \tag{2}$$

where the 2-spinors, $\chi_{\kappa m}(\theta, \varphi)$, are eigenfunctions of $\boldsymbol{j}^2$, $\boldsymbol{l}^2$, and j_z with eigenvalues of $j(j+1)\hbar^2$, $l(l+1)\hbar^2$, and $m_z\hbar$, respectively, and $P(r)$ and $Q(r)$ are the large and small radial components of the wavefunction, respectively.

For a many-body quantum system, we begin with a Slater determinant which is the antisymmetrized product of the one-electron wavefunctions in Eq. (2):

$$\psi(\mathbf{r}_1, \ldots, \mathbf{r}_N) = \frac{1}{\sqrt{N!}} \begin{vmatrix} \phi_1(\mathbf{r}_1) & \cdots & \phi_N(\mathbf{r}_1) \\ \vdots & \ddots & \vdots \\ \phi_1(\mathbf{r}_N) & \cdots & \phi_N(\mathbf{r}_N) \end{vmatrix}, \tag{3}$$

where $\mathbf{r}_n$ is the radial coordinate, $(r_n, \theta_n, \varphi_n)$, for the nth electron. For an N-electron atom the configuration state functions (CSFs), $|\gamma, J^\pi, M\rangle$, are built from linear combinations from these Slater determinants. Treating the atom as an isolated atom with no preferred axis yields eigenvalues of $\boldsymbol{J}^2$ and J_z as $J(J+1)\hbar^2$ and $M\hbar$, respectively. This assumption will be discussed in detail in Sec. VIII. The overall parity of the state is given by π, and γ represents all other quantum numbers required for the specific CSF.

Finally, a normalized linear combination of CSFs defines an atomic state function (ASF):

$$|\Gamma, J^\pi, M\rangle = \sum_{J, \gamma} C_{\Gamma, \gamma} |\gamma, J^\pi, M\rangle, \tag{4}$$

where the ASF includes all possible angular momenta, and Γ defines all other quantum numbers for the particular ASF.

So far, this only includes products of single-electron central-field orbitals. Assuming the central core of the atom is dominated by spherically symmetric closed orbitals allows this to be a good initial estimate for an iterative, self-consistent method. The Davidson algorithm is used to solve for the large and small radial components from Eq. (2), $P(r)$ and $Q(r)$, respectively [49,70]. This iterative process obtains a final wavefunction from a linear combination of CSFs with stationary energy with respect to variations in radial wavefunctions and mixing coefficients [71].

These formulas are generic for both closed or open electron shells. However, the mathematics is greatly simplified when the shells are fully occupied. For scandium, the lone $3d$ electron can exist in many quantum states, $m_\ell \in \{-2, -1, 0, 1, 2\}$, which all increase the number of spin-coupling possibilities and therefore configuration state functions. This increases the complexity and lowers the probability of obtaining convergence during the self-consistent iterative process. The approach is fully relativistic using jj coupling core wavefunctions with GRASP and the LCG-Welton self-energy [57,64,72].

Once wavefunctions are obtained for the occupied orbitals, the multiconfiguration active set approach is implemented to ensure that electron-electron correlation effects are accounted for. This method allows canonically unoccupied electron orbitals to be a part of the active set, which is to say that CSFs are included where an excitation from an occupied to an unoccupied shell is permitted. For these calculations, we allow up to two excitations from the $n \geqslant 3$ subshells into subshells $\{4p, 4d, 4f, 5s, 5p, 5d, 5f, 6s\}$. This results in a vast number of allowed CSFs but ensures convergence of the wavefunction and a small energy shift due to electron correlations. The necessity of including these excitations can be seen in Fig. 1, where excitations allowed to higher subshells provide a convergence of the wavefunctions and the energy eigenvalues. Convergence is a key metric in any self-consistent process and we explore this in greater detail in Sec. IV.
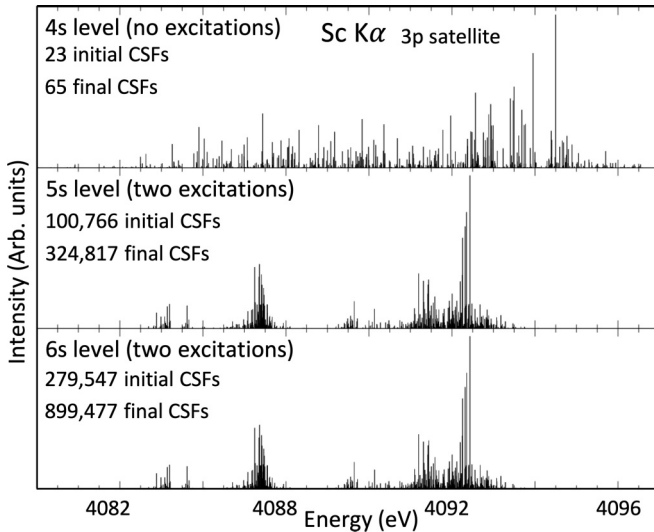
FIG. 1. The Sc $K\alpha$ $3p$ shake-off satellite ($[1s3p] \rightarrow [2p3p]$) at three different levels of expanding the active set. The numbers of configuration state functions (CSFs) in both the final and initial states are presented. The inclusion of the multiconfiguration active set expansion clearly improves the structure of the energy eigenvalue spectrum, from a spread-out, incorrect distribution of eigenvalues to a $K\alpha$ structure with two discernible peaks. Notably, there is great consistency between the $5s$ and $6s$ levels, and these spectra fit data much better than the $4s$ level of computation.

Finally, biorthogonalization of the initial and final wavefunctions allows energy eigenvalues to be obtained. The initial and final ASF for the canonical $K\alpha$ transitions are the electron configurations $\{1s^12s^22p^63s^23p^63d^14s^2\}$ and $\{1s^22s^22p^53s^23p^63d^14s^2\}$, respectively. For an nl shake-off satellite transition, an nl hole exists in both the initial and final states. The outcome is similar for $K\beta$ transitions where the $3p$ subshell relaxes into the $1s$.

III. ENERGY EIGENVALUE SPECTRA

Figures 1–9 display results for the Sc $K\alpha$ canonical, diagram, transition $[1s] \rightarrow [2p]$; seven single shake-off satellite transitions, $[1snl] \rightarrow [2pnl]$ for $nl \in \{1s, 2s, 2p, 3s, 3p, 3d, 4s\}$; and two double shake-off satellites $[1sn_1l_1n_2l_2] \rightarrow [2pn_1l_1n_2l_2]$ for $n_1l_1n_2l_2 \in \{4s4s = 4s^2, 3d4s\}$. All these results are also shown for $K\beta$ with the substitution $2p \rightarrow 3p$. For the diagram transitions in both $K\alpha$ and $K\beta$ profiles, we label several *clusters* of eigenvalues, which may offer insight when comparing different transitions. For example, in Fig. 2 the two clusters α_{21} and α_{22} defined in the diagram transitions remain clear in the $3p$ and $4s$ satellite transitions and the $4s^2$ double satellite transitions in Fig. 4. These clusters do not exist for the $3d$ and $3d4s$ satellites since they have too few eigenvalues for the separation of the α_1 or α_2 group. The near-degenerate single shake-off satellites along with the diagram transitions are presented in Figs. 2 and 3 for $K\alpha$ and $K\beta$, respectively.

The complete lists of all transitions for both $K\alpha$ and $K\beta$ transition eigenvalues are presented in the Supplemental Material [73]. The lists contain the initial and final states, the energy of the eigenvalue along with the Einstein A_L coefficient
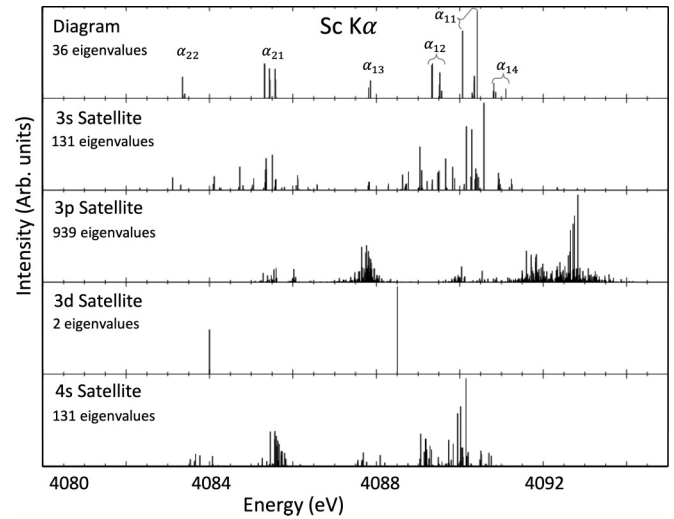
in the length gauge, the total angular momentum J number, the parity P value, and the g_f factor. The diagram lines are also presented with the cluster that each eigenvalue belongs to.

For $K\alpha$ transitions, the structure and energy of the diagram transitions are similar to the $4s$ and $3s$ satellite transitions. This leads to challenges when fitting experimental data, as the profiles overlap very closely. Dean *et al.* ([15], Fig. 15) showed the overlap between the diagram and $4s$ satellite profile which led to them not using this transition in their
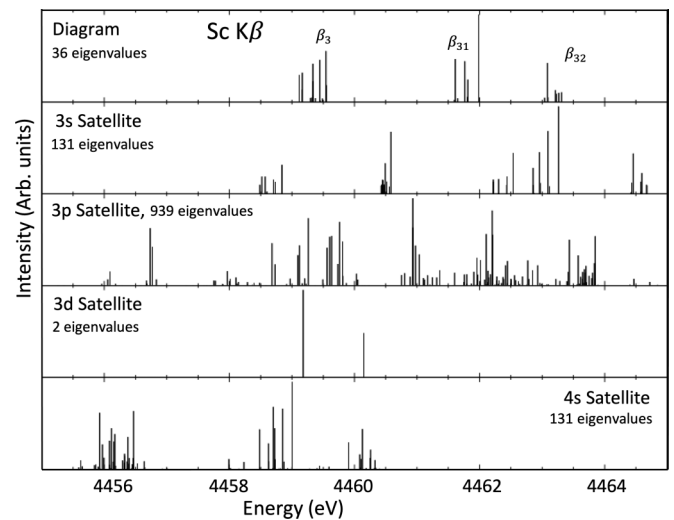

FIG. 2. Sc $K\alpha$ eigenvalue spectra for the diagram ($[1s] \rightarrow [2p]$) and near-degenerate single nl shake-off satellites ($[1snl] \rightarrow [2pnl]$). The calculations have been computed at the $6s$ level of the active set expansion. The intensities (amplitudes) are relative within each transition. For the diagram transitions, we have designated groupings of eigenvalues to different clusters which may aid in comparison with other transitions.

FIG. 3. Sc $K\beta$ eigenvalue spectra for the diagram ($[1s] \rightarrow [3p]$) and near-degenerate single nl shake-off satellites ($[1snl] \rightarrow [3pnl]$). The calculations have been computed at the $6s$ level of the active set expansion. The intensities (amplitudes) are relative within each transition. We have labeled groups of eigenvalues with a cluster identifier which may help in comparison to other transitions.
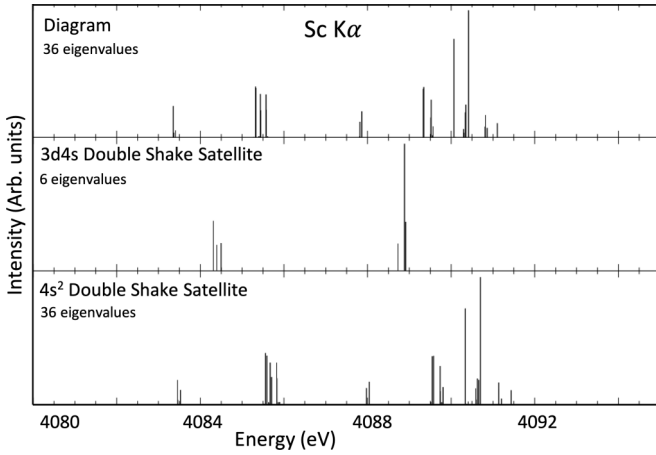
FIG. 4. Sc $K\alpha$ eigenvalue spectra for the two most dominant double shake-off satellites: $4s^2$ and $3d4s$ shake-off satellites. The diagram transitions are presented for comparison.

fitting. Transitions like these *ab initio* intensity calculations are essential and enable the fitting of the transitions, which we perform in this work.

There are several interesting features when comparing the $K\beta$ transitions to the $K\alpha$ ones. The $K\beta$ $3p$ shake-off satellite is not significantly higher in energy than the diagram, as opposed to the same satellite in $K\alpha$. The $3s$ and $4s$ satellites for $K\alpha$ are very similar to the diagram transitions, which is not the case for $K\beta$.

The near-degenerate double shake-off satellites along with the diagram line for both $K\alpha$ and $K\beta$ are presented in Figs. 4 and 5, respectively. The structure of $K\alpha$ remains intact even with the addition of these extra hole states. However, for the $K\beta$ $3d4s$ shake-off satellite transition, the β_1 and β_3 peaks become much closer in energy and the separated peak structure cannot be observed. In general, the $K\alpha$ transitions have a much clearer structure than the $K\beta$.

The separated peak structure in Sc $K\alpha$ appears to be lost when the $n = 2$ electron is shaken off in the high-energy shake-off satellites. The $n = 2$ shake-off satellites are often associated with the $K\alpha_{3,4}$ satellite and our calculations represent
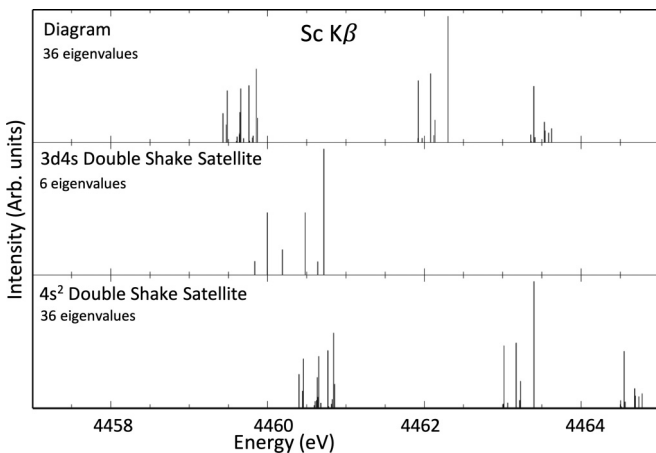

FIG. 5. Sc $K\beta$ eigenvalue spectra for the two most dominant double shake-off satellites, together with the diagram line.
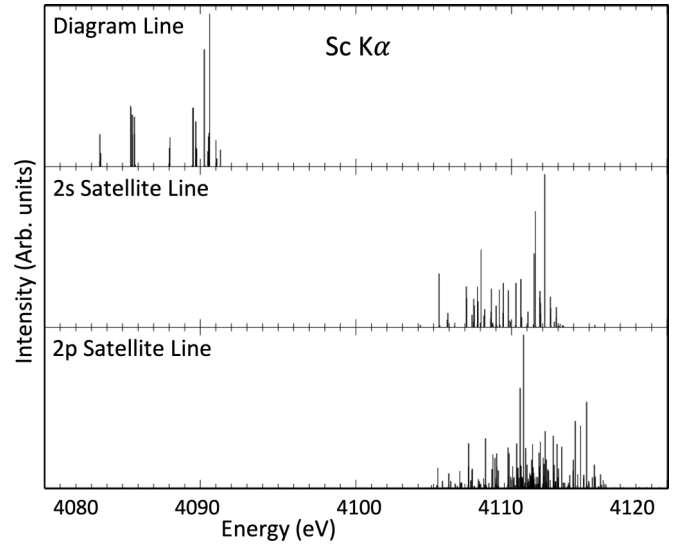

FIG. 6. Sc $K\alpha$, eigenvalue spectra for the $n = 2$ shake-off satellites which are responsible for the $K\alpha_{3,4}$ satellite in the $3d$ transition metals. The diagram transitions have been presented for comparison. There is no clear $K\alpha_1$ and $K\alpha_2$ structure present in these spectra.

a prediction since these transitions have not been observed using photonic incident energy. Some scandium multiple hole transitions have been observed, including the $n = 2$ shake-off satellite, but from heavy ion (30 MeV) bombardment and not photonic (x-ray) perturbation [74]. Recent work on the $K\alpha_{3,4}$ spectrum in copper has shown that our MCDHF process can obtain accurate eigenvalue spectra that fit the best high-resolution experimental data well [60,75]. Figure 6 gives the eigenvalue spectra for the $n = 2$ shake-off satellites, or the $K\alpha_{3,4}$ satellite. The $K\beta$ counterpart is presented in Fig. 7. For the $3d$ transition metals, the $K\beta$ $n = 2$ shake-off satellite is often close in energy to the valence to core $K\beta_{2,5}$, $3d \rightarrow 1s$, forbidden transition [28]. Studies of the $K\beta$ $n = 2$ satellite
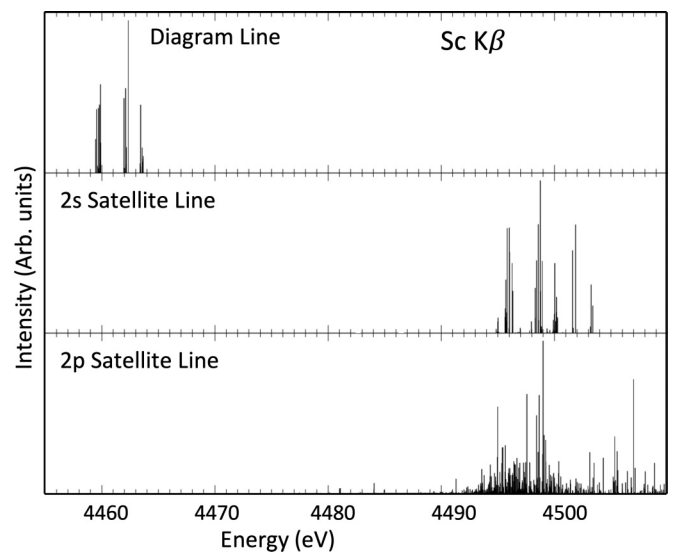

FIG. 7. Sc $K\beta$ $n = 2$ shake-off satellites and the diagram transitions for comparison. These transitions overlap with the valence-to-core $K\beta_{2,5}$ transition ($[1s] \rightarrow [3d]$), which means theoretical calculations are necessary for resolving the two transitions.
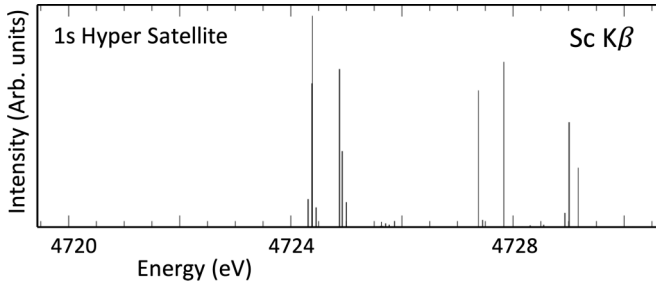
FIG. 8. Sc $K\alpha$ double $1s$ ionization hypersatellite ($K\alpha^h$) spectrum. As with the $n = 2$ satellites for $K\alpha_{3,4}$, no empirical data exist for this transition. A previous result for this transition reported a single energy rather than an eigenvalue spectrum; the two results are within 1 eV of this work's peak energy [77].

are therefore important for parsing between the two different transitions when they overlap.

The final eigenvalue spectra determined herein are for the $1s$ shake-off satellite transitions, often called hypersatellites, $K\alpha^h$ and $K\beta^h$ in other $3d$ transition metals. As with the $n = 2$ shake-off satellites, these have not been observed in scandium with photonic incident energy. These are presented in Figs. 8 and 9 for $K\alpha$ and $K\beta$, respectively.

Costa *et al.* have presented theoretical calculations using multiconfiguration Dirac-Fock theory [76,77]. These were reported as a single value from the statistical average of all the transitions, rather than presenting the full spectrum of eigenvalues. Their work presents the energies as the shift from the diagram line, which we assume is the value taken from Deslattes *et al.* [38]. Their value for Sc $K\alpha_1^h = 4306.84$ eV compares incredibly well with ours of Sc $K\alpha^h = 4306.51$ eV. However, we do not distinguish between the splitting of $K\alpha_1^h$ and $K\alpha_2^h$ in this work, which is a topic for future work since we observe the breakdown of strict α_1 and α_2 structure, which is not observed in the previous work by Costa *et al.* [76,77].

For Sc $K\beta^h$, Costa *et al.* report an energy of 4729.59 eV, which is roughly 3 eV greater than our statistical average of 4726.80. Unlike $K\alpha$, Costa *et al.* do not make the distinction between $K\beta_1^h$ and $K\beta_3^h$. Overall, more work is needed on the hypersatellites of all $3d$ transition metals, scandium included. However, this requires new high-precision and well-resolved experimental data first.
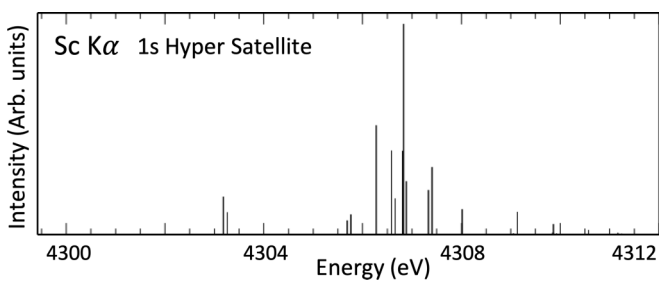

FIG. 9. Sc $K\beta$ double $1s$ ionization hypersatellite ($K\beta^h$) spectrum. As with the $n = 2$ satellites, no empirical data exist for this transition. Similar to the $K\alpha^h$ spectrum, the Sc $K\beta^h$ has previously been presented with theoretical calculations obtaining a single value, rather than a spectrum of eigenvalues, and that result is within 3 eV of this work's peak energy [76].

IV. CONVERGENCE CRITERIA

GRASP uses an iterative process minimizing the Dirac Hamiltonian, which requires convergence with the self-consistent field (SCF) approach [49,50,57]. The expansion of the active set begins with the ASF produced by only considering the ground-state CSFs up to the $4s$ level; then wavefunctions are built, allowing two excitations from the ground-state orbitals into some nl shell, $nl \in \{4p, 4d, 4f, 5s, 5p, 5d, 5f, 6s\}$. Therefore, we investigate two meanings of convergence: the convergence of a single wavefunction during the SCF approach, and the convergence of eigenvalues as the active set is expanded.

To determine convergence for a single wavefunction, the ratio of the Einstein A coefficient calculated in two gauges is presented and values close to unity indicate a good level of convergence. The two gauges chosen are the length (Babushkin) and velocity (Coulomb) gauges, with ratio A_L/A_V. This gauge freedom should have no impact on physical observables, so the closer to unity the A_L/A_V ratio is, the greater confidence we have in the convergence of the wavefunction during the SCF procedure.

Convergence during the expansion of the active set can be done regarding several key metrics. For tests of convergence between calculations during the active set expansion, our key metrics are the shift in the peak (most intense) energy eigenvalue and the shift across all energy eigenvalues. These can be done qualitatively by qualitative observation of the shift in energy eigenvalues as in Fig. 1 or quantitatively. In the case of shifts of a large number of energy eigenvalues a center-of-mass (weighted mean) approach is useful. It enables a single value to encompass an effective energy shift, using information from every eigenvalue, but with stronger weighting for the more intense eigenvalues. We present the change in the center-of-mass energy eigenvalues as a function of active set expansion for each calculated transition in Fig. 10 for the $K\alpha$ transitions. The $K\beta$ equivalent is presented in the Supplemental Material [73]. According to this metric, typical incremental convergence is 0.02 to 0.09 eV for all $K\alpha$ and $K\beta$ satellites. While most transitions appear to converge consistently towards a smaller change as the active set is expanded, the $1s$, $2s$, $2p$, and $3d4s$ diverge between 0.02 and 0.08 eV at the $5f$ to $6s$ level. The reasons for this are not yet clear and are a source for future work. Other than the $3d4s$ double shake-off satellite, the three transitions that feature this divergence are the complex inner shell shake-off transitions. Other work has found similar issues with convergence for these transitions in copper $K\alpha$ [28], and could perform calculations to higher levels of the active set. However, scandium with its $3d$ lone electron adds many spin-coupling states, increasing the computational requirements for each active set expansion and we are unable, at present, to run calculations up to greater than the $6s$ expansion.

There are many more metrics one can use and that are critical for demonstrating convergence and we present a comprehensive summary in the Supplemental Material [73]. We include tables of the shift in center-of-mass energy from the $5s$ to the $6s$ expansion; the shift in the peak (greatest g_f) energy from the $5s$ to the $6s$ expansion level; the weighted mean A_L/A_V ratios from the $4s$ to $6s$ expansion level; the A_L/A_V
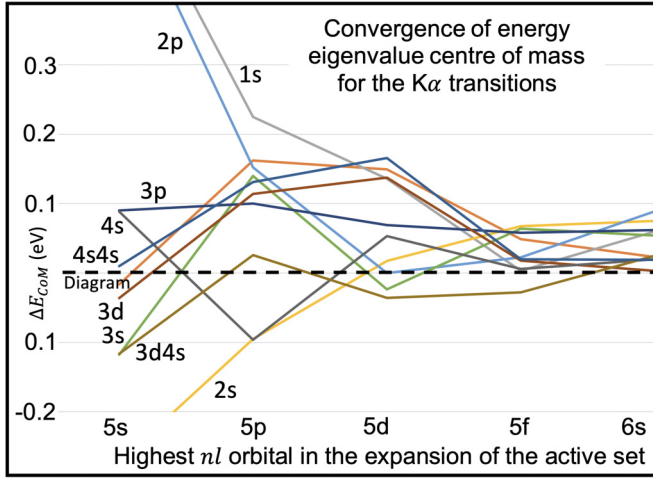
FIG. 10. This figure plots the energy shift, ΔE_{CoM}, of the center of mass energy for the energy eigenvalue spectra for the $K\alpha$ transitions. In the equation $\Delta E_{CoM}(nl) = E_{CoM}(nl) - E_{CoM}(n_-l_-)$, the nl value represents the x axis as the orbital that the active set has been expanded to, and n_-l_- represents the previous level. All transition center-of-mass energies have been plotted, with the label nl representing the nl shake-off satellite, and $nlnl$ representing a double shake-off satellite.

ratios for the peak eigenvalue from the $4s$ to $6s$ expansion level; and the fractional change in the intensity factor, g_f. All of these are presented in the Supplemental Material [73].

There is a significant change in the energies from the $4s$ to the $4f$ expanded active set levels, resulting in shifts an order of magnitude larger than from $4f$ to $6s$ levels of expansion, and, therefore, we typically leave the $4s$ to $4f$ shift out of the plots. Typically, the energy convergences are between 0.01 and 0.1 eV, peak and weighted mean; A_L/A_V ratios are between 0.7% and 3.8%; and the g_f factors converge between 1% and 3%. The $K\alpha$ results are usually better than the $K\beta$ results which is consistent with other similar studies and supports later claims when fitting results are better for $K\alpha$ than $K\beta$.

The A_L/A_V ratio is an important test of convergence but is more meaningful when paired with the fractional change in just one of the gauges since the A_L/A_V ratio may hide significant movements in the two values. The fractional change in the A_L coefficient is introduced as a weighted mean for each transition from the $4f$ to the $6s$ expansion level.

We may also consider the change in the intensities as the expansion of the active set is performed. These values range over orders of magnitude depending on the intensity of the eigenvalue; therefore, we consider ratio of each eigenvalue's g_f at the nl expansion level to the previous, n_-l_-.

These convergence tests result in 11 tables in the Supplemental Material [73], five for $K\alpha$ and six for $K\beta$.

V. AUGER PROCESSES

An excited state atomic system can relax via the emission of a photon (radiative relaxation), an electron (nonradiative relaxation), or a combination of the two, usually referred to as a radiative Auger emission. Previous work has shown

the importance of calculating the ratios of nonradiative to radiative rates to correctly map the shake-off probabilities to satellite intensities [60]. The Cu $K\alpha_{3,4}$ satellite spectrum has had several works that calculate energy eigenvalues which agree with the experimental values for energy [21,28]. However, the shape of the Cu $K\alpha_{3,4}$ spectrum is not modeled well by theoretical predictions, which suggests that the *ab initio* intensities calculated from shake-off probabilities are incorrect [21,28,78]. This issue was resolved by Melia *et al.* after performing *ab initio* Auger rate calculations to determine an *Auger suppression factor* [60]. This suppression factor uses rate calculations to determine the probability that an nl shake-off event leads to an nl shake-off satellite, the $[2pnl] \rightarrow [1snl]$ transition, or if the nl hole is filled by an Auger process *before* the $K\alpha$ transition takes place, therefore not observing the shake-off satellite.

Due to the importance of these values in copper $K\alpha_{3,4}$, we perform similar calculations for scandium but for the near-degenerate shake-off holes, $n \in \{3, 4\}$. The radiative and nonradiative rates for these satellites are presented in Table I. The nonradiative, Auger, emission rates are calculated through the RATIP program, which is used in conjunction with GRASP [79,80]. The name given for the Auger transitions follows standard IUPAC notation where the first letter represents the initial hole orbital, the second is for the original orbital of the relaxing electron, and the last represents the orbital of the ejected electron.

Table I shows that the Auger decay channels for the $[1s3p]$ or $[1s3d]$ initial states are tiny. However, the $[1s3s]$ initial state has an Auger decay rate of $0.074 \, \text{eV}/\hbar$ and a radiative $K\alpha$ $3s$ shake-off satellite transition rate of $0.086 \, \text{eV}/\hbar$. Therefore, we expect the *ab initio* $3s$ shake-off probability to be overestimating the shake-off satellite intensity and we must reduce the satellite intensity by an *Auger suppression factor*. This is due to the $3s$ orbital hole in the $[1s3s]$ initial hole state having approximately the same probability to be filled by an Auger emission before the $K\alpha$ transition as the $K\alpha$ transition taking place with the $3s$ vacancy present. The Auger suppression factor for the $3s$ shake-off satellite is taken by dividing the radiative rate by the sum of both radiative and nonradiative rates: $0.086/(0.086 + 0.074) = 0.538$, which is unitless. For each of the fits the new, Auger-corrected value for the satellite intensities will be used.

VI. SHAKE-OFF PROBABILITIES AND SATELLITE INTENSITIES

Each x-ray profile is composed of several individual transitions, the diagram, and nl shake-off satellites. To recreate experimental spectra from the energy eigenvalue spectra presented in the previous section, the relative intensities of each transition must be calculated. Shake-off events have been proposed as the source of satellite transitions in x-ray data and many energy eigenvalue calculations exist [15,18,20,27,28,33–35,41,81–83]. However, *ab initio* calculations of shake-off probabilities are rare within the literature [25–28,78,84]. More work in both energy eigenvalues and relative intensities must be done before a good understanding of anomalous asymmetries can be claimed.

TABLE I. Calculated rates for radiative (photon emission) and nonradiative (Auger electron emission) processes for transitions involving a shake-off event (secondary ionization) from the $n = 3$ and $4s$ orbitals. These values lead to an Auger suppression factor which must be multiplied by the calculated shake-off satellite probabilities to better calculate an *ab initio* shake-off satellite intensity. The Auger suppression factor multiplies the values of *ab initio* shake-off probabilities to determine the *ab initio* satellite intensity.

Initial hole(s)	Final hole(s)	Type	Name	Rate (eV/$\hbar$)
[1s]	[2p]	Radiative	$K\alpha$ diagram	0.342
[1s3s]	[2p3s]	Radiative	$K\alpha$ 3s satellite	0.086
[1s3s]	[1s3p3d]	Nonradiative	$M_1 M_{2,3} M_{4,5}$	0.030
[1s3s]	[1s3p4s]	Nonradiative	$M_1 M_{2,3} N_1$	0.021
[1s3s]	[1s3d4s]	Nonradiative	$M_1 M_{4,5} N_1$	0.015
[1s3s]	[1s4s4s]	Nonradiative	$M_1 N_1 N_1$	0.008
		Total M_1 (3s) Auger rate: 0.074		
[1s3p]	[2p3p]	Radiative	$K\alpha$ 3p satellite	0.162
[1s3p]	[1s3d4s]	Nonradiative	$M_1 M_{2,3} M_{4,5}$	< 0.001
		Total $M_{2,3}$ (3p) Auger rate: < 0.001		
[1s3d]	[2p3d]	Radiative	$K\alpha$ 3d satellite	0.119
[1s3d]	[1s4s4s]	Nonradiative	$M_{4,5} N_1 N_1$	< 0.001
		Total $M_{4,5}$ (3d) Auger rate: < 0.001		

Mukoyama and Taniguchi performed early calculations for shake-off probability using nonrelativistic wavefunctions and other approximations [78]. Kochur *et al.* provided similar equations for their shake-off probabilities with more recent computations [84]. These studies used the adiabatic approximation, which assumes that the ejection of the core $(1s)$ electron occurs suddenly and without interaction with the rest of the wavefunction. The post- and pre-ionization wavefunctions are identical other than the loss of the core electron; however, post-ionization the wavefunction is no longer in an eigenstate of the new Hamiltonian. Therefore, the immediate post-ionization wavefunction relaxes into an eigenstate of the post-ionization Hamiltonian and during this relaxation process there is a nonzero probability that a second electron is ejected into the continuum. Experimental characteristic *reference spectra* should be measured within this adiabatic limit, where the perturbing energy far exceeds the edge energy.

Let the states φ_i be eigenstates of the ground-state, pre-ionization, atomic Hamiltonian, H. For some perturbation ionizing the atom in the adiabatic, or sudden, limit the Hamiltonian will shift immediately to some post-ionization Hamiltonian, H'. The adiabatic assumption results in the system remaining in state φ_i which is not an eigenstate of the new Hamiltonian, H'. Rather, if the eigenstates of the new Hamiltonian are φ'_i the initial states can be represented as an expansion over the new states:

$$|\varphi_i\rangle = \sum_j c_{ij} |\varphi'_j\rangle = \sum_j \langle \varphi'_j | \varphi_i \rangle |\varphi'_j\rangle, \quad (5)$$

where $c_{ij} = \langle \varphi'_j | \varphi_i \rangle$ represents the probability for the system in an initial state, φ_i, to be in a new state φ'_j after the sudden change of the Hamiltonian. So the overlap integral between the original, neutral-atom wavefunction and the new, ionized wavefunction is the necessary matrix element. The overlap integral is calculated from the large and small radial components from Eq. (2), which are outputs from GRASP. A single hole in the 1s orbital represents the canonical ionization before a $K\alpha$ transition representing the diagram lines, where a

doubly ionized wavefunction where the hole states are $[1s, nl]$ represents the probability of an nl shake-off. The wavefunctions are computed using the MCDHF method as outlined in the previous section. The shake-off probability is defined such that the sum of all shake events and the diagram (no shake) equals unity. This results in a correspondence between shake-off probability and the resulting satellite line intensity relative to the full spectrum.

This method requires an atomic wavefunction for each initial and final ASF which can be cumbersome and time-consuming. Nguyen *et al.* proposed an approach requiring only two wavefunctions, the neutral atom and the $[1s]$ ion [28,28]. Their equation is written with the κ quantum number, $\kappa = (l - j)(2j + 1)$:

$$p_{n\kappa} = \frac{1}{M_{n\kappa}} \left(1 - \left| \sum_j c_j d_j \langle \varphi_{Bn\kappa} | \varphi_{An\kappa} \rangle^{Mjn\kappa} \right|^2 \right), \quad (6)$$

where $p_{n\kappa}$ is the probability of shake-off per electron in the $n\kappa$ state, $M_{n\kappa}$ is the number of electrons in the $n\kappa$ state, and c_j and d_j are the mixing coefficients for the two states. Equation (6) overlooks the possibility for two or more electrons to be removed, so, in order to obtain the specific number of shake-off events during a transition, the binomial theory is used to obtain Eq. 29 from Ref. [28]:

$$P(X = k) = \binom{M_{n\kappa}}{k} \left(1 - (1 - p_{n\kappa})^{\frac{1}{M_{n\kappa}}}\right)^k (1 - p_{n\kappa})^{\frac{M_{n\kappa} - k}{M_{n\kappa}}}, \quad (7)$$

where $P(X = k)$ is the probability that k electrons are removed from the $n\kappa$ state. This equation has been derived from the same starting equation as our Eq. (5) and, therefore, should obtain similar results. Very similar values are achieved for single shake-off probabilities. For completeness, we present our results with results from both Eqs. (5) and (7) in Table II.

Table II contains our *ab initio* shake-off probabilities derived using both Eqs. (5) and (7); the values provided by Mukoyama and Taniguchi [78] and Kochur *et al.* [84]; and the values obtained through semiempirical means from Dean *et al.* [15]. Dean *et al.* calculated the energy eigenvalues of the

TABLE II. Results of semiempirical derived shake-off probabilities and theoretical *ab initio* shake-off probabilities. There is good consistency between the *ab initio* results but the semiempirical results are all larger than the theoretical ones. Taken as satellite intensities, the percentages are relative to the full spectrum. Methods of Eqs. (5) and (7) agree closely except for the double shake-off events. We recommend using values from Eq. (5).

nl shake-off (%)	[1s]	[2s]	[2p]	[3s]	[3p]	[3d]	[4s]	[3d4s]	[4s²]
Semiempirical results using Sc $K\alpha$ experimental data									
Dean *et al.* [15,31]				2	13	10			
Semiempirical results using Sc $K\beta$ experimental data									
Dean *et al.* [15,32]				3	13	18	2		
ab initio Theory									
Mukoyama and Taniguchi [78]	0.006	0.194	1.016	0.936	7.76	4.98	15.16		
Kochur *et al.* [84]		0.37	1.81	1.75	9.14	6.01			
This work [Eq. (7)]	0.192	0.366	1.51	1.32	8.80	6.46	16.1	0.596	1.43
This work [Eq. (5)]	0.188	0.357	1.60	1.21	8.74	6.58	16.5	0.783	1.85
Normalized satellite intensities including Auger suppression									
nl shake-off satellite intensity (%)				Diagram		[3s]	[3p]	[3d]	[4s]
Eq. (5) with Auger suppression and renormalized				65.31		0.684	9.12	6.91	17.3

diagram transitions and the $n = 3$ and $4s$ satellite transitions. Using experimental data [31,32], they fit the eigenvalue spectra with free intensities, and the best fit normalized intensity was offered as the semiempirical shake-off probability. Difficulties in resolution meant they could not fit the $4s$ shake-off for the $K\alpha$ data, and the $K\beta$ value is much smaller than expected. There is a decent agreement with both theory and the two experiments with the $3s$ and $3p$ shake-off intensities. But the semiempirical $3d$ shake-off intensity is much larger than expected and not consistent between the two experimental data sets.

VII. COMPARISON WITH EXPERIMENT

Having defined and demonstrated a high level of convergence, we now investigate the validity of these theoretical results by comparing to experimental data. Three data sets exist which would make suitable comparison with the presented theoretical calculations, those of Anagnostopoulos *et al.* [33], Ito *et al.* [34,35], and Dean *et al.* [31,32]. The highest resolution data for Sc $K\alpha$ [31] and Sc $K\beta$ [32] are within the 1σ uncertainties of the other two [33–35], which indicates that the same conclusions for the validity of fitting should be achieved regardless of the data set chosen. The Dean *et al.* data set is an absolute measurement whereas the other two are relative measurements. Furthermore, the Dean *et al.* data sets contain well-defined experimental errors with an uncertainty of 2 parts per million, or 0.01 eV for $K\alpha$, and 0.009 eV for $K\beta$. For these reasons, we compare to the Dean *et al.* data set.

The shake-off satellite intensities used for the fitting of the theory are presented in the last row of Table II. These are the same as the shake-off probabilities from Table II except for the $3s$ shake-off satellite intensity since this is now multiplied by the Auger suppression factor.

A subshell resolved transition, t, is the spectrum of eigenvalues for a diagram, or nl shake-off satellite, so $t \in \{\text{Diagram}, 3s, 3p, 3d, 4s\}$. The eigenvalues within each transition are the fine-structure resolved eigenvalues. The eigenvalue spectra for a given subshell resolved transition, t, create a profile by assigning each n energy eigenvalue with a

Lorentzian profile, $L_n(E_n, c_n, \gamma_t)$, the peak energy, E_n, being the n energy eigenvalue, the area being the relative intensity of the eigenvalue, c_n, and the full width at half maximum (FWHM), γ, being a constant for each eigenvalue within the transition. Each of these Lorentzian profiles will be summed to achieve a profile for the particular transition. The c_n in this equation is the normalized intensity of each n eigenvalue in the spectrum.

The model, I_t, for each subshell-resolved transition, t, containing N total eigenvalues is therefore

$$I_t(E; \gamma_t) = \sum_{n=1}^{N} L(E_{n,t}, c_{n,t}; \gamma_t). \tag{8}$$

And the full spectrum, composed of the diagram transitions and nl shake-off satellite transitions is the sum of each I_t with relative amplitude, A_t

$$I(E) = \sum_t A_t I_t(E; \gamma_t), \tag{9}$$

where A_t is the intensity of each transition taken from the last row of Table II. So Eq. (8) represents the spectrum created within one panel of Fig. 2, and Eq. (9) represents the spectrum when adding the spectrum from each panel in the same figure.

We make conclusions regarding the effectiveness of recreating the spectrum with *ab initio* methods using χ^2 reduced (χ_r^2) goodness-of-fit measures and F-tests. Fitting to experiment expects the need for fitting parameters. The energy shift parameter, ΔE_t, and intensity scaling parameter, ΔA_t, are the two parameters we consider and are included for each transition:

$$I(E) = \sum_t A_t(1 + \Delta A_t)I_t(E + \Delta E_t; \gamma_t). \tag{10}$$

The models in this work have the Lorentzian width, γ_t, as a free parameter. This work aims to investigate the ability of MCDHF theory to calculate from first principles the shake-off satellite intensities and the eigenvalue energy spectra. Hereinafter, widths will be free parameters.
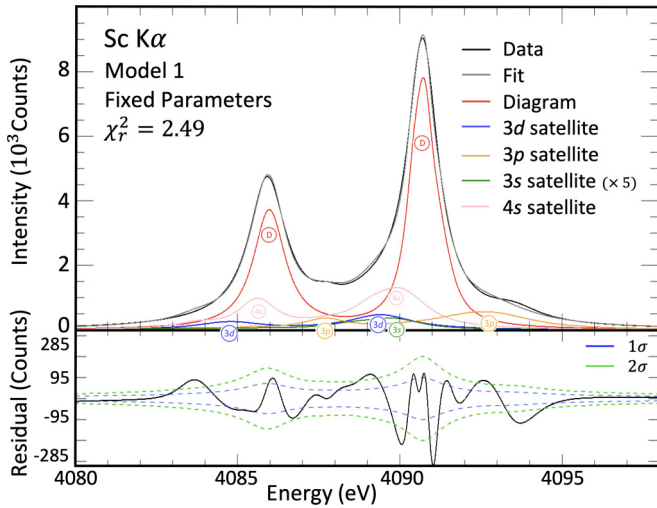
FIG. 11. Model 1 for Sc $K\alpha$, where only the Lorentzian FWHM and Gaussian experimental width are free parameters. The $K\alpha''$ feature is seen roughly 3 eV greater than the $K\alpha_1$ and the $3p$ satellite energy is roughly 1 eV too low to fit this well as suggested by Shigeoka *et al.* [85]. Circular labels are placed under the α_1 and α_2 peaks to aid in distinguishing. Only one peak is labeled for the $3s$ satellite since it has very low intensity and is very spread out with no obvious two-peak structure. The goodness-of-fit measure obtains $\chi_r^2 = 2.49$.

By fitting the calculated eigenvalue spectra and intensities to experiment for Sc $K\alpha$ and $K\beta$ with only widths as free parameters, we obtain χ_r^2 of 2.49 and 3.29, respectively (Fig. 11 for $K\alpha$ and Fig. 13 for $K\beta$). This represents a successful fit in the field of x-ray spectra of complex open-shell atomic systems.
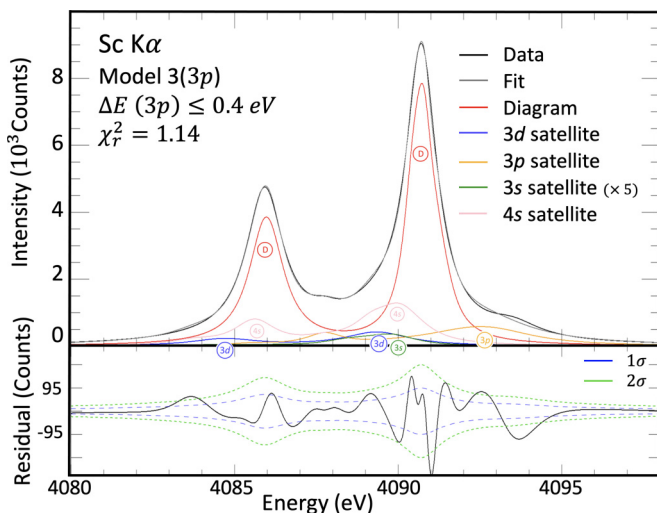

FIG. 12. Model 3($3p$), allowing only the $3p$ satellite energy to shift by at most 0.4 eV. There is a notable improvement in χ_r^2 from 2.49 to 1.14 compared with the model with all parameters fixed to theoretical prediction, with the addition of only one extra free parameter allowing the $K\alpha''$ satellite to be better accounted for. This is our recommended model. The same circular labels as Fig. 11 are provided to aid in discerning the different satellites.
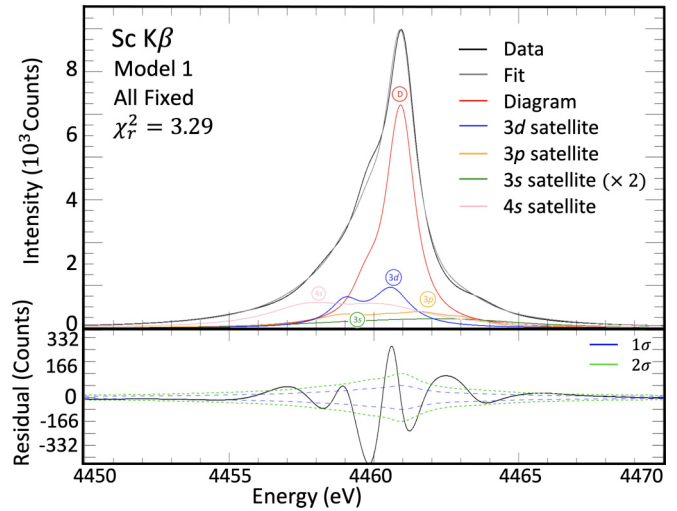

FIG. 13. The Sc $K\beta$ profile with the fitting of model 1 where the diagram and four shake-off satellite intensities and energies are fixed to the *ab initio* theory.

To help determine the validity of our calculated shake-off probabilities and energy eigenvalues, we perform the fitting with several models. The parameters that we either alter or fix are the energy shift parameter, ΔE_t, and intensity scaling parameter, ΔA_t. Model 1 keeps all parameters, other than widths, fixed to theoretical predictions. Model 2 keeps the energy eigenvalues fixed to theory ($\Delta E = 0$), while allowing the area, A_t (shake-off probabilities), to be free. Model 3 allows energies to shift from theoretical predictions, while fixing area to theoretical predictions ($\Delta A = 0$). Model 4 enables widths, energies, and probabilities to be free parameters. We include models that only allow one transition's parameters to be free and in these instances follow the model number by the transition in parentheses. For example, keeping everything fixed except allowing the $K\alpha$ $3p$ shake-off satellite energy eigenvalues to shift ($\Delta E_{3p} \neq 0$) is labeled model 3($3p$).

Each eigenvalue energy shift is allowed to shift by up to 0.4 eV ($K\alpha$) or 0.5 eV ($K\beta$), corresponding to the local convergence level up to 0.09 eV and noting that the $K\beta$ theoretical spectra show weaker convergence. Similarly, theoretical convergence criteria for intensities and probabilities at 0.7% to 2.4% ($K\alpha$) or 1.0% to 3.8% ($K\beta$) suggest possible intensity limitations of theory at up to the 5% level. Hence we expect, if there are significant changes to eigenvalue or intensity, that they lie within these limits.

The results of these models are given in Secs. VII A and VII C. Presented are the values of ΔE, ΔA, the FWHM, and the χ_r^2. Plots of the fits are also shown for the fixed models, model 1, and the *best* model which is chosen through a Fisher F-test, in Sec. VII B.

A. Sc $K\alpha$

Figures 11 and 12 present two of the $K\alpha$ models, and results for ΔE, ΔA, the FWHM, and the χ_r^2 for all models are presented in Table III.

TABLE III. Results of five different key models for the $K\alpha$ spectrum, with the shifts in energy and intensity relative to the *ab initio* theory, the fitted widths, and χ_r^2. The satellite transitions are referenced just by their nl shake-off orbital.

$K\alpha$ model	Parameter	Diagram	[3s]	[3p]	[3d]	[4s]	χ_r^2
1	ΔA (%)						
All fixed	ΔE (eV)						2.49
Fig. 11	FWHM (eV)	1.18	3.28	2.01	1.49	2.36	
2	ΔA (%)	−0.32	+0.06	+2.43	+0.50	−4.64	
$\Delta A \leqslant 5\%$	ΔE (eV)						1.57
	FWHM (eV)	1.25	3.12	2.54	1.64	2.13	
3(3p)	ΔA (%)						
$\Delta E_{3p} \leqslant 0.4$ eV	ΔE (eV)			+0.39			1.14
Fig. 12	FWHM (eV)	1.18	3.21	1.97	1.55	2.07	
3	ΔA (%)						
$\Delta E \leqslant 0.4$ eV	ΔE (eV)	+0.14	−0.05	+ 0.36	−0.27	−0.35	0.83
	FWHM (eV)	1.06	3.09	1.87	1.57	2.39	
4	ΔA (%)	−0.22	+ 0.04	+1.03	+0.46	−4.23	
Both $\Delta A \leqslant 5\%$	ΔE (eV)	+0.08	−0.02	+ 0.31	−0.29	−0.14	0.76
and $\Delta E \leqslant 0.4$ eV	FWHM (eV)	1.24	2.90	1.91	1.64	2.04	

Importantly, model 1 shows significant limitations in four spectral regions:

(1) Around the $K\alpha_1$ peak, 4090.5 eV, there is a particular combination of amplitude and width error, possibly due to the diagram spectrum, the $4s$ satellite, or other satellite spectral limitations.

(2) Around the $K\alpha''$ feature, 4092.5–4093.5 eV, the model particularly suggests that the $3p$ satellite feature is too low in energy and too broad in width.

(3) A peak around 4087.5 eV only appears on deconvolution, perhaps relating to the $3p$ satellite or due to the deconvolution.

(4) The absence of a peak around 4083.5 eV is possibly related to the $4s$ or $3d$ satellite structure or correlated shifts.

If we permit the intensities to vary within an assumed possible uncertainty from our *ab initio* theory, model 2, with five extra free parameters, ten total, we obtain $\chi_r^2 = 1.58$, superior to all previous work. Instead, if the intensities are fixed to theory but the energies may shift with model 3 (ten free parameters) then the fit has $\chi_r^2 = 0.83$. This fit is extremely favorable over model 2. We also defined model 4 where both energies and intensities vary, with a total of 15 free parameters and the best fit, $\chi_r^2 = 0.76$.

A χ_r^2 less than one suggests possible overfitting. So we have defined model 3(3p) which only lets the $3p$ shake-off satellite energy shift. The eigenvalues for the $3p$ satellites shift by 0.39 eV and the fit, $\chi_r^2 = 1.14$, is far superior to both the earlier semiempirical fits and theoretical fits. This defines a portable standard for experiments and is presented in Fig. 12.

A larger parameter shift may yield an improved χ_r^2, but may be nonphysical and suggests a deficiency of theory or experiment or the comparability of the two. For the Sc $K\alpha$ fits, parameter shifts are bounded by $|\Delta E| \leqslant 0.4$ eV, and $|\Delta A| \leqslant 0.05$, or 5%. Both of these are plausibly physical given the convergence achieved in the wavefunctions. Having many free parameters allows a low χ_r^2 given the data accuracies. However, so many parameters may be neither physical nor meaningful.

B. Fisher F-tests for Sc $K\alpha$ modeling

As the models include more free parameter shifts of eigenvalue or amplitude compared with theoretical prediction, the χ_r^2 lowers. However, does this demonstrate a better model, or is it simply a byproduct of including more (possibly nonphysical) free parameters? We use Fisher F-tests to compare these different models. F-tests and related measures are based on the above-mentioned χ^2 and χ_r^2 and the degrees of freedom and changes of degrees of freedom. The F-test is said to pass, signifying that the new model is a better representation of data than the previous, if the F statistic is greater than the critical value of the F distribution for some level of confidence. The F statistic is

$$F = \frac{\Delta\chi^2 N_{\text{dof}}}{\chi^2 \Delta p}, \qquad (11)$$

where N_{dof} is the number of degrees of freedom in the model, and Δp is the difference in the number of free parameters between the two models. Since the F-test is a comparative test, we compare all models to model 1 where all parameters are fixed and it gives a χ_r^2 of 2.49 and a nonreduced χ^2 of 2563. Table IV presents the F statistic and the relevant critical F value for the given comparison. The strongest model is the one not only with the best fit represented by the smallest χ_r^2 but also the best ansatz, which is often demonstrated by having fewer free parameters in the fitting function.

Table IV shows that the F statistic is greater than the critical F value for all the models, indicating they are all better theoretical models for the data to the null hypothesis case of all parameters being fixed. An F-test tests directly between a base model and models that have more free parameters. One can interpret the ratio between the critical F value and the F statistic as an indication of *how* successful a model has been, and in this way have a measure of significance between two models. However, it is cleaner to perform the F-test directly between these other models which is why comparisons are also made between model 2 and model 4, between

TABLE IV. Results of the comparative F-test between model 1 and the other four models for the $K\alpha$ spectrum and model 2 with model 4; model 3($3p$) with models 3 and 4; and model 3 with model 4. Model 3($3p$), where all values are fixed to *ab initio* theory except the $3p$ shake-off satellite energy eigenvaluesm provides the strongest model hypothesis.

$K\alpha$	Critical F value	F statistic
Model 2 to 1	10.1	70.9
Model 3 to 1	10.1	129
Model 3($3p$) to 1	10.6	526
Model 4 to 1	9.7	67.4
Model 2 to 4	4.56	5.09
Model 3($3p$) to 3	7.88	4.21
Model 3($3p$) to 4	7.56	0.93
Model 3 to 4	4.56	6.85

model 3($3p$) and models 3 and 4, and between model 3 and model 4.

Overall, the Sc $K\alpha$ spectrum has been well modeled with *ab initio* theory with only a width-free parameter, with $\chi_r^2 = 2.49$. Including only one extra free parameter and letting the $3p$ shake-off satellite energy to shift by $+0.39$ eV results in a remarkable fit of $\chi_r^2 = 1.14$. This strongly supports the MCDHF approach for reconstructing x-ray spectra for complex open-shell atoms.

C. Sc $K\beta$

The method for obtaining fits and comparing them to the experiment is the same for the Sc $K\beta$ profile. In Fig. 13, model 1 is presented as the case with only widths as free parameters, and in Fig. 14, model 3 (all energies free) is presented as the most successful model according to the F-test. All tested models have their F-test scores when compared to model 1, and all models are superior to model 1. As with $K\alpha$, some select comparisons are shown in Table VI which are even
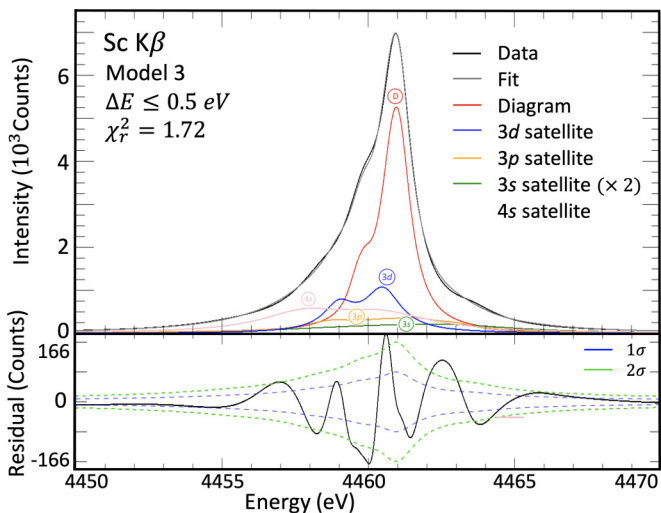

FIG. 14. The Sc $K\beta$ profile with the fitting of model 3 where all transition energies are allowed to shift by up to 0.5 eV. This is the best model according to the Fisher F-test (Table VI).

more important for the $K\beta$ profile since there is no clear best-performing F-test model as in the $K\alpha$ case.

More models are tested for $K\beta$ than $K\alpha$ since with $K\alpha$ there was an obvious choice in allowing the $3p$ satellite profile shift in energy which led to the 3($3p$) model and a better fit of the $K\alpha''$ feature. This is not the same for $K\beta$. It is much less obvious what shifts, or scales, should obtain a low χ_r^2 and a suitable ansatz with as few free parameters as possible. Therefore, in addition to all the $K\alpha$ models, we include models 3($3d$) and 3(D) in which only the $3d$ or diagram transitions, respectively, are allowed to shift. There is no strong candidate for the best model, with model 3($3d$), model 3(D), and model 3 all showing roughly the same ratio of F statistic to F value. The results of ΔA, ΔE, and FWHM for all seven models are presented in Table V.

None of the models describes the spectrum for $K\beta$ to the same level of precision as achieved for $K\alpha$. This is consistent with all other work in the literature which finds that *ab initio* calculations of $K\alpha$ spectra for transition metals are more accurate than their $K\beta$ counterparts. What is not obvious is which model is the best when considering the desire for as few free parameters as possible. Models 3, 3(D), and 3($3d$) all have the same order of magnitude in the ratio between the critical F value and the F statistic with model 3 being slightly better. This suggests that the energy has not converged as well for the $K\beta$ transitions as it has for $K\alpha$, which is supported when considering the convergence criteria in Sec. IV and the values in the Supplemental Material [73].

We suggest that for future studies of the Sc $K\beta$ spectrum, the model values are used for portable spectral parameters.

D. Raw data modeling

These results are extremely promising. However, most researchers should ask if their theory or models apply to the actual experimental data, i.e., the nondeconvolved spectra. To ensure the effectiveness of using theoretical models to recreate realistic data with nonzero Gaussian width we fit our theoretical models to the raw data for Sc $K\alpha$ and $K\beta$ from Refs. [31] and [32], respectively.

We have performed the fit by replacing the Lorentzian profiles from Eqs. (8)–(10) with Voigt profiles. A Voigt profile is the convolution between a Lorentzian and a Gaussian. All models have undergone this process with the extra fitting parameter of Gaussian width. The F-tests have been recalculated and show no change in which model provides the best fit in Table VII. Figures 15 and 16 present the fits to raw data for $K\alpha$ and $K\beta$, respectively. The values of the fitting parameters are presented in Table VIII.

VIII. DISCUSSION

The greatest source of error in the $K\alpha$ fits appears to come from discrepancies around the $K\alpha''$ peak. This is the small shoulder in the data roughly 3 eV higher than the main $K\alpha_1$ peak. This feature has been observed in several experiments for $3d$ transition metals and is larger in lower-Z elements [85,86]. The satellite was hypothesized to originate from the $3p$ shake-off satellite by Scott [87]. Our theoretical calculations and fits reinforce this view, due to the $3p$ satellite

TABLE V. Results of seven different fitting models for the $K\beta$ spectrum. Presented are the shifts in energy, intensity, and the fitted widths along with the χ_r^2 goodness-of-fit measure. Some models fit better than others. However, a formal F-test is presented in Table VI to determine which model is superior. The satellite (sat.) transitions are referenced by their nl shake-off orbital.

$K\beta$		Transition					
model	Parameter	Diagram	$3s$ sat.	$3p$ sat.	$3d$ sat.	$4s$ sat.	χ_r^2
1	ΔA (%)						
All Fixed	ΔE (eV)						3.29
figure 13	FWHM (eV)	1.35	2.58	2.28	1.75	2.53	
2	ΔA (%)	-0.32	$+0.02$	$+2.43$	$+0.35$	-4.89	
$\Delta A \leqslant 5\%$	ΔE (eV)						2.53
	FWHM (eV)	1.43	3.04	2.29	1.64	2.03	
3	ΔA (%)						
$\Delta E \leqslant 0.5$ eV	ΔE (eV)	$+0.34$	-0.24	$+0.43$	$+0.04$	-0.45	1.72
figure 14	FWHM (eV)	1.26	2.87	1.99	1.57	2.08	
$3(3p)$	ΔA (%)						
$\Delta E_{3p} \leqslant 0.5$ eV	ΔE (eV)			$+0.44$			3.17
	FWHM (eV)	1.22	2.97	2.31	1.14	1.89	
$3(3d)$	ΔA (%)						
$\Delta E_{3d} \leqslant 0.5$ eV	ΔE (eV)				-0.27		3.01
	FWHM (eV)	1.35	3.00	2.20	1.37	1.94	
$3(D)$	ΔA (%)						
$\Delta E_D \leqslant 0.5$ eV	ΔE (eV)	$+0.42$					2.27
	FWHM (eV)	1.39	3.15	2.34	1.48	2.24	
4	ΔA (%)	-0.22	$+0.04$	$+2.35$	$+0.28$	-4.35	
$\Delta A \leqslant 5\%$							
$\Delta E \leqslant 0.5$ eV	ΔE (eV)	$+0.08$	$+0.06$	$+0.19$	-0.29	-0.20	1.52
	FWHM (eV)	1.30	2.74	1.97	1.85	1.93	

eigenvalue spectra being roughly 3 eV greater than the diagram line (Fig. 2) and the fits showing the $3p$ satellite around the same location as the $K\alpha''$ peak. The importance in testing

TABLE VI. Results of the comparative F-test between models. More models are considered for the $K\beta$ spectrum as we do not have such a strong, and obvious, candidate as with model $3(3p)$ in the $K\alpha$ case. Model 3, where energy eigenvalues are free to shift, provides the strongest model, but not by much over model $3(D)$, where only the diagram shifts in energy. Other than comparing all models to model 1, comparisons are made between models 2 and 4, between models 3 and 4; and between models $3(m)$ and models 3 and 4, where $m \in \{3p, 3d, D\}$, for D the diagram.

$K\beta$	Critical F value	F statistic
Model 2 to 1	10.1	44.8
Model 3 to 1	10.1	92.6
Model $3(3p)$ to 1	10.6	35.4
Model $3(3d)$ to 1	10.6	82.6
Model $3(D)$ to 1	10.6	91.4
Model 4 to 1	9.7	52.2
Model 2 to 4	4.56	5.23
Model $3(3p)$ to 3	7.88	12.07
Model $3(3d)$ to 3	7.88	9.51
Model $3(D)$ to 3	7.88	7.72
Model $3(3p)$ to 4	7.56	5.28
Model $3(3d)$ to 4	7.56	17.89
Model $3(D)$ to 4	7.56	20.34
Model 3 to 4	4.56	12.42

model $3(3p)$ highlighted this issue and resulted in this model being the best, by far, to model the data with.

Shigeoka *et al.* performed calculations and experiments for titanium ($Z = 22$) where the semiempirical intensity was found to be 2.5% and the *ab initio* shake-off probability was 6.5% [85]. The *ab initio* value is slightly smaller than our obtained value of 8.74% and semiempirical value is much smaller than ours of 9.77% using model 4 where all parameters were free.

TABLE VII. Results of the F-test for all models for both $K\alpha$ and $K\beta$ when applied to raw data and using Voigt profiles as opposed to Lorentzian profiles. The results are consistent with the results for the deconvolved data.

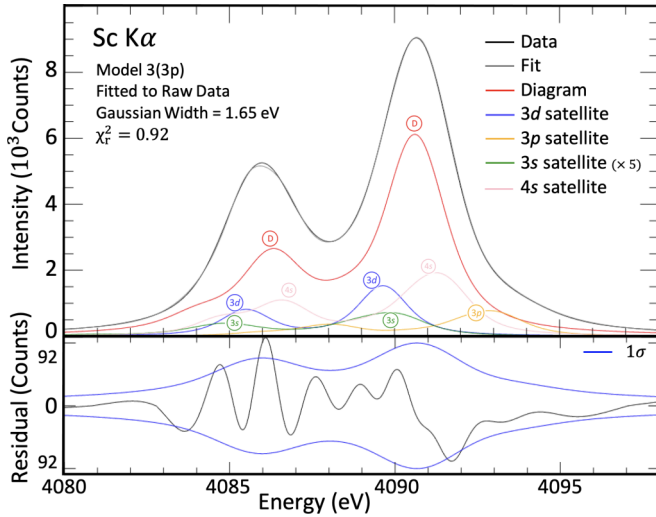| Raw $K\alpha$	Critical F value	F statistic
Model 2	10.6	76.5
Model 3	10.6	138
Model $3(3p)$	11.0	552
Model 4	10.1	73.0
Raw $K\beta$	Critical F-value	F-statistic
Model 2	10.6	49.0
Model 3	10.6	100.2
Model $3(3p)$	11.0	38.3
Model $3(3d)$	11.0	89.4
Model $3(D)$	11.0	96.8
Model 4	10.1	58.1

FIG. 15. Model 3($3p$) fitted to the raw spectral data of Dean *et al.* [31]. The Gaussian width is 1.65 eV. The addition of the Gaussian width ensures all residuals are within 2σ of error and almost all are within 1σ.
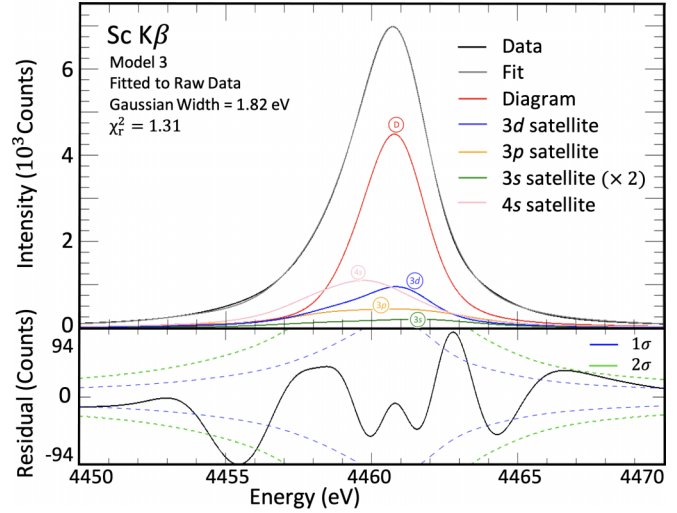

FIG. 16. Scandium $K\beta$ model 3 fitted to raw spectral data [32]. The Gaussian width is 1.82 eV. The addition of the Gaussian width decreases the χ_r^2 to 1.31 and almost all of the residuals are within 2σ of the fit.

From experimental work, the $K\alpha''$ intensity is seen to decrease across the group of $3d$ transition metals. For example, the copper $K\alpha''$ intensity is obtained with a semiempirical intensity of 0.5% by Deutsch *et al.* [18] and the *ab initio* value is 4.49% by Nguyen *et al.* [28]. The work on *ab initio* intensities for the $K\alpha''$ feature in $3d$ transition metals is incomplete as not all elements have had theoretical intensities calculated. This work provides a calculation for this value in scandium and also supports the hypothesis that the origin of the feature is in the $3p$ shake-off satellite.

There is some debate on the validity of using atomic physics theory to match data taken from metal solids. The main concern is that, due to the presence of other charges, the assumption that the Dirac equation is the one presented in Eq. (1) with a central field potential and therefore has solutions of the form in Eq. (2) is incorrect. This critique is particularly weak since the vast body of research that uses the Dirac-Hartree-Fock approach to fit data of metal solid x-ray fluorescence spectra has consistently shown a remarkable level of precision and accuracy. Recently [60], it was shown that MCDHF calculations can replicate the Cu $K\alpha_{3,4}$ satellite spectra to within 0.25 eV with satellite intensity in agreement with data. This work, too, has shown how MCDHF

calculations achieve a fit for the Sc $K\alpha$ spectrum of $\chi_r^2 = 1.14$ where only the energy of the $3p$ satellite shifts by 0.39 eV.

Therefore, we can say with certainty that the MCDHF approach recreates experimental results to within the current experimental resolution for $K\alpha$ spectra. Perhaps, as transitions between outer shells are studied, we will see a divergence from this since external charges will impact outer shells more than inner orbitals. Atomic theory can predict the experimental results from metal solids for $K\alpha$ transitions to within current experimental accuracy.

The Sc $K\alpha_{3,4}$ satellite and Sc $K\alpha^h$ hypersatellite have only been observed with high-energy incident ionic perturbations with a low-resolution detector [74]. Some recent experiments on hypersatellites in the $3d$ transition metals exist [88,89], yet there are no works for scandium. This work provides calculations for these spectra with the $n = 1, 2$ shake-off satellite eigenvalue spectra. Future work in this area would require a measurement of these spectra and Auger suppression calculations which affect inner shell intensities far more than outer shells.

$K\beta$ theoretically derived energies and intensities have been fitted to experimental data to obtain $\chi_r^2 = 1.72$ with only one

TABLE VIII. The parameters of the most successful models when fitting to the raw, nondeconvolved, data.

Raw data fits	Parameter	Transition						
		Diagram	$3s$	$3p$	$3d$	$4s$	χ_r^2	Gaussian FWHM (eV)
Kα	ΔA (%)							
Model 3($3p$)	ΔE (eV)			$+0.35$			0.92	1.65
Fig. 15	Lorentzian FWHM (eV)	1.22	2.36	2.05	1.83	2.31		
Kβ	ΔA (%)							
Model 3	ΔE (eV)	$+0.32$	-0.28	$+0.41$	$+0.07$	-0.31	1.31	1.82
Fig. 16	Lorentzian FWHM (eV)	1.21	2.53	1.80	1.77	2.13		

free energy parameter with model 3 and five free widths. Similar to $K\alpha$, this represents an achievement comparable to any other studies of $K\alpha$ spectra. That the Kβ does not fit the data as well as the $K\alpha$ raises interesting questions about the fundamental physics that differentiates between the two.

The $K\beta$ transitions involve the $3p$ orbital and this may be more suspected from solid-state effects due to the smaller shielding. The greatest source of error in the fitting for $K\alpha$ came from the $3p$ shake-off satellite and the $K\alpha''$ shoulder. In the $K\beta$ spectrum, there is also a shoulder on the high-energy side of the peak and in keeping consistent notation we should refer to it as the $K\beta''$ satellite. However, in the $K\beta$ energy eigenvalue calculations, the $3p$ shake-off satellite does not have a peak with higher energy than the diagram line. Therefore, the Kβ'' shoulder is not fitted well in the theoretical model. There are convergence issues with the Kβ $3p$ shake-off satellite which do not occur for the $K\alpha$ which may be due to the $K\beta$ transition with a $3p$ spectator vacancy having a double vacancy in this shell.

Similar to $K\alpha$, the $n = 1, 2$ shake-off satellites have not been observed for scandium with incident photonic energy. However, for $K\beta$, the $n = 2$ shake-off satellite has an overlapping valence-to-core transition which results in the $K\beta_{2,5}$ spectral profile [90].

IX. CONCLUSION

We have performed multiconfiguration Dirac-Hartree-Fock calculations to recreate the $K\alpha$ and $K\beta$ x-ray spectra of scandium. To do so, energy eigenvalue spectra of the canonical, diagram, transition $[1s] \rightarrow [2p]$ $(K\alpha)$ and $[1s] \rightarrow [3p]$ $(K\beta)$, and four nl shake-off satellites with $nl \in \{3s, 3p, 3d, 4s\}$ were calculated. To determine the relative intensity of these transitions, the *ab initio* shake-off probabilities were calculated with an Auger suppression factor to take into account the possibility for nonradiative relaxation. These values have led to the successful modeling of both deconvolved and raw data. To ensure good ansatz and to prevent overfitting, Fisher F-tests were performed for the several different models used for fitting. Ultimately, we present model $3(3p)$ with only one free energy parameter in the $3p$ satellite as the successful model for $K\alpha$ with a goodness-of-fit $\chi_r^2 = 1.14$. The $K\beta$ spectrum has been modeled with model 3 where each transition has a free energy parameter and $\chi_r^2 = 1.72$. The fits were also applied to the raw data, with the inclusion of a Gaussian broadening term, and resulted in $\chi_r^2 = 0.92$ $(K\alpha)$ and $\chi_r^2 = 1.31$ $(K\beta)$.

The current standard for characteristic x-ray spectra for the scandium $K\alpha$ and $K\beta$ transitions has, therefore, been recreated to high accuracy and precision by *ab initio* calculations. Further to the fitting of extant data, this work has presented several eigenvalue spectra and theoretical shake-off probabilities for transitions not observed with photonic incident energy. This represents a prediction that future experimental work should test.

This work has presented an extensive array of tests of convergence that have not been used elsewhere for MCDHF calculations of electronic wavefunctions. These include the center-of-mass energy shift, the peak eigenvalue energy shift, the A_L/A_V ratio as both a center-of-mass value and for the peak eigenvalue, and the weighted mean g_f. The metrics are essential to obtaining a lower bound on uncertainty calculations as well as showing confidence in the successful calculation of a well-converged electron wavefunction, important for an iterative process such as the MCDHF method with the active set expansion approach. Most of these tables and figures are presented in the Supplemental Material [73]. We would recommend all future MCDHF calculations that employ the expansion of the active set to include similar checks of convergence.

The claim that the $K\alpha''$ satellite arises from the $3p$ shake-off has been demonstrated and the hypothesis that its intensity reduced across the $3d$ transition metals group is supported. Furthermore, the necessity of expanding the active set is demonstrated especially for transitions with a large number of eigenvalues.

The need for accurate *ab initio* calculations in x-ray physics is important in tests of advanced quantum mechanics, atomic physics, and quantum electrodynamics. Determining the x-ray spectra of species that are not well known experimentally leads to improved future experiments where knowing the energy range for experiment can be calculated beforehand, or when removing noise from certain impurities. The two strongest models we have provided will serve as a benchmark for theoretical x-ray spectra for scandium and the methods described will be extended to other $3d$ transition metals.

[1] A. Beyer, L. Maisenbacher, A. Matveev, R. Pohl, K. Khabarova, A. Grinin, T. Lamour, D. C. Yost, T. W. Hänsch, N. Kolachevsky, and T. Udem, Science **358**, 79 (2017).

[2] P. M. Carvalho, S. Pessanha, J. Machado, A. L. Silva, J. Veloso, D. Casal, D. Pais, and J. P. Santos, Spectrochim. Acta, Part B **174**, 105991 (2020).

[3] X. Feng, H. Zhang, and P. Yu, Crit. Rev. Food Sci. Nutr. **61**, 2340 (2021).

[4] B. Beckhoff, Nanomaterials **12**, 2255 (2022).

[5] I. Y. Silachyov, J. Anal. Chem. **75**, 878 (2020).

[6] L. Musílek, R. Prokeš, and T. Trojek, Radiat. Phys. Chem. **200**, 110388 (2022).

[7] V. K. Garg, A. L. Srivastav, M. K. Tiwari, A. Sharma, and V. S. Kanwar, J. Environ. Treat. Tech. **9**, 192 (2021).

[8] M. Siegbahn and W. Stenstrom, Phys. Z. **17**, 318 (1916).

[9] G. Wentzel, Ann. Phys. **66**, 84 (1921).

[10] M. J. Druyvesteyn, Z. Phys. **43**, 707 (1927).

[11] D. Coster and M. J. Druyvesteyn, Z. Phys. **40**, 765 (1927).

[12] F. X. Richtmyer, J. Franklin Inst. **208**, 325 (1929).

[13] F. Bloch, Phys. Rev. **48**, 187 (1935).

[14] T. Åberg, Phys. Rev. **156**, 35 (1967).

[15] J. W. Dean, P. Pushkarna, H. A. Melia, T. V. B. Nguyen, and C. T. Chantler, J. Phys. B **55**, 075002 (2022).

[16] W. C. Sauder, J. R. Huddle, J. D. Wilson, and R. E. Lavilla, Phys. Lett. A **63**, 313 (1977).

[17] M. Deutsch and M. Hart, Phys. Rev. B **26**, 5558 (1982).

[18] M. Deutsch, G. Hölzer, J. Härtwig, J. Wolf, M. Fritsch, and E. Förster, Phys. Rev. A **51**, 283 (1995).

[19] M. Deutsch, O. Gang, K. Hamalainen, and C. C. Kao, Phys. Rev. Lett. **76**, 2424 (1996).

[20] G. Hölzer, M. Fritsch, M. Deutsch, J. Härtwig, and E. Förster, Phys. Rev. A **56**, 4554 (1997).

[21] M. Fritsch, C. C. Kao, K. Hämäläinen, O. Gang, E. Förster, and M. Deutsch, Phys. Rev. A **57**, 1686 (1998).

[22] R. Diamant, S. Huotari, K. Hämäläinen, C. C. Kao, and M. Deutsch, Phys. Rev. Lett. **84**, 3278 (2000).

[23] S. Galambosi, H. Sutinen, A. Mattila, K. Hämäläinen, R. Sharon, C. C. Kao, and M. Deutsch, Phys. Rev. A **67**, 022510 (2003).

[24] C. T. Chantler, A. C. L. Hayward, and I. P. Grant, Phys. Rev. Lett. **103**, 123002 (2009).

[25] J. A. Lowe, C. T. Chantler, and I. P. Grant, Phys. Rev. A **83**, 060501(R) (2011).

[26] T. L. H. Pham, T. V. B. Nguyen, J. A. Lowe, I. P. Grant, and C. T. Chantler, J. Phys. B **49**, 035601 (2016).

[27] T. V. B. Nguyen, H. A. Melia, F. I. Janssens, and C. T. Chantler, Phys. Lett. A **426**, 127900 (2022).

[28] T. V. B. Nguyen, H. A. Melia, F. I. Janssens, and C. T. Chantler, Phys. Rev. A **105**, 022811 (2022).

[29] H.-B. Qin, S. Yang, M. Tanaka, K. Sanematsu, C. Arcilla, and Y. Takahashi, Chem. Geol. **552**, 119771 (2020).

[30] A. B. Botelho, D. C. R. Espinosa, and J. A. S. Tenório, Chem. Geol. **38**, 161 (2021).

[31] J. W. Dean, H. A. Melia, C. T. Chantler, and L. F. Smale, J. Phys. B **52**, 165002 (2019).

[32] J. W. Dean, C. T. Chantler, L. F. Smale, and H. A. Melia, J. Phys. B **53**, 205004 (2020).

[33] D. F. Anagnostopoulos, R. Sharon, D. Gotta, and M. Deutsch, Phys. Rev. A **60**, 2018 (1999).

[34] Y. Ito, T. Tochio, H. Ohashi, M. Yamashita, S. Fukushima, M. Polasik, K. Slabkowska, L. Syrocki, E. Szymańska, J. Rzadkiewicz, P. Indelicato, J. P. Marques, M. C. Martins, J. P. Santos, and F. Parente, Phys. Rev. A **94**, 042506 (2016).

[35] Y. Ito, T. Tochio, M. Yamashita, S. Fukushima, A. M. Vlaicu, L. Syrocki, K. Slabkowska, E. Weder, M. Polasik, K. Sawicka, P. Indelicato, J. P. Marques, J. M. Sampaio, M. Guerra, J. P. Santos, and F. Parente, Phys. Rev. A **97**, 052505 (2018).

[36] J. A. Bearden and A. F. Burr, Rev. Mod. Phys. **39**, 125 (1967).

[37] J. A. Bearden, Rev. Mod. Phys. **39**, 78 (1967).

[38] R. D. Deslattes, E. G. Kessler, P. Indelicato, L. de Billy, E. Lindroth, and J. Anton, Rev. Mod. Phys. **75**, 35 (2003).

[39] S. I. Bokarev and O. Kühn, WIREs Comput. Mol. Sci. **10**, e1433 (2020).

[40] B. N. C. Tenorio, T. A. Voss, S. I. Bokarev, P. Decleva, and S. Coriani, J. Chem. Theory Comput. **18**, 4387 (2022).

[41] V. G. Yarzhemsky and L. V. Chernysheva, J. Phys. B **55**, 165002 (2022).

[42] X. Liu, Y. Shi, X. Li, F. Lu, Y. Wang, H. Hu, and Y. Luo, J. Phys. B **55**, 125001 (2022).

[43] A. N. Hopersky, A. M. Nadolinsky, and S. A. Novikov, Phys. Rev. A **98**, 063424 (2018).

[44] J. W. Fowler, B. K. Alpert, D. A. Bennett, W. B. Doriese, J. D. Gard, G. C. Hilton, L. T. Hudson, Y. I. Joe, K. M. Morgan, G. C. O'Neil, C. D. Reintsema, D. R. Schmidt, D. S. Swetz, C. I. Szabo, and J. N. Ullom, Metrologia **54**, 494 (2017).

[45] J. S. Schelfhout and J. J. McFerran, Phys. Rev. A **104**, 022806 (2021).

[46] J. S. Schelfhout and J. J. McFerran, Phys. Rev. A **105**, 022805 (2022).

[47] M. Bilal, A. V. Volotka, R. Beerwerth, and S. Fritzsche, Phys. Rev. A **97**, 052506 (2018).

[48] N. Aourir, M. Nemouchi, M. Godefroid, and P. Jönsson, Phys. Rev. A **97**, 032506 (2018).

[49] C. Froese Fischer, T. Brage, and P. Jönsson, *Computational Atomic Structure: An MCHF Approach* (Institute of Physics, London, 1997).

[50] I. P. Grant, *Relativistic Quantum Theory of Atoms and Molecules: Theory and Computation* (Springer, Berlin, 2007).

[51] L. Wu, J. Jiang, Z.-W. Wu, Y.-J. Cheng, G. Gaigalas, and C.-Z. Dong, Phys. Rev. A **106**, 012810 (2022).

[52] N. M. Hosea, J. Jose, and H. R. Varma, J. Phys. B **55**, 135001 (2022).

[53] Y. Guo, A. Borschevsky, E. Eliav, and L. F. Pašteka, J. Phys. B **55**, 155003 (2022).

[54] C. Zhang and L. Cheng, J. Phys. Chem. A **126**, 4537 (2022).

[55] M. Guerra, J. M. Sampaio, T. I. Madeira, F. Parente, P. Indelicato, J. P. Marques, J. P. Santos, J. Hoszowska, J. C. Dousse, L. Loperetti, F. Zeeshan, M. Müller, R. Unterumsberger, and B. Beckhoff, Phys. Rev. A **92**, 022507 (2015).

[56] Y. Ménesguen, M.-C. Lépy, P. Hönicke, M. Müller, R. Unterumsberger, B. Beckhoff, J. Hoszowska, J.-C. Dousse, W. Błachucki, Y. Ito, M. Yamashita, and S. Fukushima, Metrologia **55**, 56 (2018).

[57] C. Froese Fischer, G. Gaigalas, P. Jönsson, and J. Bieron, Comput. Phys. Commun. **237**, 184 (2019).

[58] P. Jönsson, G. Gaigalas, C. F. Fischer, J. Bieroń, I. P. Grant, T. Brage, J. Ekman, M. Godefroid, J. Grumer, J. Li, and W. Li, Atoms **11**, 68 (2023).

[59] P. Jönsson, M. Godefroid, G. Gaigalas, J. Ekman, J. Grumer, W. Li, J. Li, T. Brage, I. P. Grant, J. Bieroń, and C. F. Fischer, Atoms **11**, 7 (2023).

[60] H. A. Melia, J. W. Dean, T. V. B. Nguyen, and C. T. Chantler, Phys. Rev. A **107**, 012809 (2023).

[61] J. Li, G. Gaigalas, J. Bieroń, J. Ekman, P. Jönsson, M. Godefroid, and C. Froese Fischer, Atoms **10**, 132 (2022).

[62] Y. Li, P. Jönsson, M. Godefroid, G. Gaigalas, J. Bieroń, J. P. Marques, P. Indelicato, and C. Chen, Atoms **11**, 4 (2023).

[63] I. Angeli and K. Marinova, At. Data Nucl. Data Tables **99**, 69 (2013).

[64] T. Nguyen, J. Lowe, T. Pham, I. Grant, and C. Chantler, Radiat. Phys. Chem. **204**, 110644 (2023).

[65] J. A. Lowe, C. T. Chantler, and I. P. Grant, Radiat. Phys. Chem. **85**, 118 (2013).

[66] M. Guidon, J. Hutter, and J. VandeVondele, J. Chem. Theory Comput. **5**, 3010 (2009).

[67] M. Bender, P. Heenen, and P. Reinhard, Rev. Mod. Phys. **75**, 121 (2003).

[68] R. Sure and S. Grimme, J. Comput. Chem. **34**, 1672 (2013).

[69] J. Caillat, J. Zanghellini, M. Kitzler, O. Koch, W. Kreuzer, and A. Scrinzi, Phys. Rev. A **71**, 012712 (2005).

[70] A. Stathopoulos and C. F. Fischer, Comput. Phys. Commun. **79**, 268 (1994).

[71] D. R. Hartree, W. Hartree, and B. Swirles, Philos. Trans. R. Soc. London A **238**, 229 (1939).

[72] C. T. Chantler, T. V. B. Nguyen, J. A. Lowe, and I. P. Grant, Phys. Rev. A **90**, 062504 (2014).

[73] See Supplemental Material at http://link.aps.org/supplemental/10.1103/PhysRevA.109.022809 for all convergence critera tables and figures.

[74] B. Hodge, R. Kauffman, C. F. Moore, and P. Richard, J. Phys. B **6**, 2468 (1973).

[75] M. H. Mendenhall, A. Henins, L. T. Hudson, C. I. Szabo, D. Windover, and J. P. Cline, J. Phys. B **50**, 115004 (2017).

[76] A. M. Costa, M. C. Martins, J. P. Santos, P. Indelicato, and F. Parente, J. Phys. B **39**, 2355 (2006).

[77] A. M. Costa, M. C. Martins, J. P. Santos, P. Indelicato, and F. Parente, J. Phys. B **40**, 57 (2007).

[78] T. Mukoyama and K. Taniguchi, Phys. Rev. A **36**, 693 (1987).

[79] S. Fritzsche, J. Electron Spectrosc. Relat. Phenom. **114-116**, 1155 (2001).

[80] S. Fritzsche, Comput. Phys. Commun. **183**, 1525 (2012).

[81] Y. Ito, T. Tochio, H. Oohashi, and A. M. Vlaicu, Radiat. Phys. Chem. **75**, 1534 (2006).

[82] K. S. Srivastava, R. L. Shrivastava, O. K. Harsh, and V. Kumar, Phys. Rev. B **19**, 4336 (1979).

[83] S. Doniach and M. Sunjic, J. Phys. C **3**, 285 (1970).

[84] A. G. Kochur, A. I. Dudenko, and D. Petrini, J. Phys. B **35**, 395 (2002).

[85] N. Shigeoka, H. Oohashi, T. Tochio, Y. Ito, T. Mukoyama, A. M. Vlaicu, H. Yoshikawa, and S. Fukushima, Phys. Scr. **T115**, 1080 (2005).

[86] L. Parratt, Phys. Rev. **49**, 132 (1936).

[87] B. L. Scott, Phys. Rev. A **34**, 4438 (1986).

[88] Y.-P. Maillard, J.-C. Dousse, J. Hoszowska, M. Berset, O. Mauron, P.-A. Raboud, M. Kavčič, J. Rzadkiewicz, D. Banaś, and K. Tökési, Phys. Rev. A **98**, 012705 (2018).

[89] J. Hoszowska, A. K. Kheifets, J. C. Dousse, M. Berset, I. Bray, W. Cao, K. Fennane, Y. Kayser, M. Kavčič, J. Szlachetko, and M. Szlachetko, Phys. Rev. Lett. **102**, 073006 (2009).

[90] F. Zeeshan, J. Hoszowska, J.-C. Dousse, D. Sokaras, T.-C. Weng, R. Alonso-Mori, M. Kavčič, M. Guerra, J. M. Sampaio, F. Parente, P. Indelicato, J. P. Marques, and J. P. Santos, X-Ray Spectrom. **48**, 351 (2019).